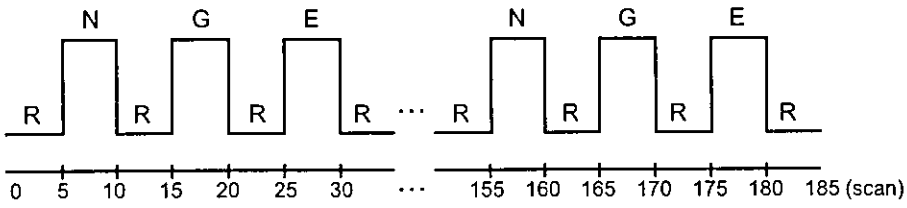

Fig. 1. Block design paradigm in the fMRI study. R = rest, N = neutral, G = guilt, E = embarrassment.

participants viewed a crosshair pattern projected to the center of the screen. In each 20-s block, five different sentences of the same emotional class were presented for 4 s each. After the scan, subjects rated the described situations according to how guilty or embarrassing they seemed using a 6-point analog scale.

Image acquisition

Images were acquired with a 1.5-T Signa system (General Electric, Milwaukee, WI). Functional images of 185 volumes were acquired with T2*-weighted gradient echo planar imaging sequences sensitive to the blood oxygenation level dependent (BOLD) contrast. Each volume consisted of 40 transaxial contiguous slices with a slice thickness of 3 mm to cover almost the whole brain (flip angle, 90°; TE, 50 ms; TR, 4 s; matrix, 64 × 64; field of view, 24 × 24 cm). High-resolution, T1-weighted anatomic images were acquired for anatomic comparison (124 contiguous axial slices, 3D Spoiled-Grass sequence (SPGR), slice thickness 1.5 mm, TE, 9 ms; TR, 22 ms; flip angle, 30°; matrix, 256 × 192; field of view, 25 × 25 cm).

Analysis of functional imaging data

Data analysis was performed with statistical parametric mapping software package (SPM99) (Wellcome Department of Cognitive Neurology, London, UK) running with MATLAB (Mathworks, Natick, MA). All volumes were realigned to the first volume of each session to correct for subject motion and were spatially normalized to the standard space defined by the Montreal Neurological Institute (MNI) template. After normalization, all scans had a resolution of 2 × 2 × 2 mm^3. Functional images were spatially smoothed with a 3D isotropic Gaussian kernel (full width at half maximum of 8 mm). Low frequency noise was removed by applying a high-pass filter (cutoff period = 240 s) to the fMRI time series at each voxel. A temporal smoothing function was applied to the fMRI time series to enhance the temporal signal-to-noise ratio. Significant hemodynamic changes for each condition were examined using the general linear model with boxcar functions convoluted with a hemodynamic response function. Statistical parametric maps for each contrast of the t statistic were calculated on a voxel-by-voxel basis. The t values were then transformed to unit normal distribution, resulting in Z scores.

To assess the specific condition effect, we used the contrasts of guilt minus neutral (G − N) and embarrassment minus neutral (E − N). A random effects model, which estimates the error variance for each condition across subjects, was implemented for group analysis. This procedure provides a better generalization for the population from which data are obtained. The contrast images were obtained from single-subject analysis and were entered into the group analysis. A one-sample t test was applied to determine group activation for each effect. Significant clusters of activation were determined using the conjoint expected probability distribution of the height and extent of Z scores with the height ($Z > 3.09$; $P <$

Table 2
Brain activation in guilt condition and embarrassment condition relative to neutral condition

Brain region	Coordinates			BA	Z score	Voxels
	x	y	z			
Guilt minus neutral						
L visual cortex (cuneus, LG)	−6	−95	12	17,18,19	4.55	1114
R visual cortex (LG)	2	−85	6	17,18	5.41	
L MPFC (MFG, SFG)	−16	49	9	6,8,9,10	4.7	1175
R MPFC (MFG)	4	57	16	9,10	3.62	
L posterior STS (MTG)	−44	−61	20	39	4.4	210
Embarrassment minus neutral						
L visual cortex (cuneus, LG, FG)	−2	−89	4	17,18,19	4.91	4343
R visual cortex (cuneus, LG)	20	−70	0	17,18	5.52	
L MPFC (MFG, SFG)	−8	50	25	6,8,9,10	4.44	840
R MPFC (MFG, SFG)	2	59	17	9,10	3.75	
L posterior STS (MTG, STG)	−42	−59	18	39	4.24	185
L middle temporal cortex (MTG)	−51	−31	−7	21	4.56	132
L anterior temporal cortex (MTG)	−53	1	−24	21	4.3	50
R anterior temporal cortex (MTG, FG)	48	−7	−27	20	3.69	44
L OFC (IFG)	−44	31	−7	47	3.68	36
L hippocampus	−34	−18	−18		3.85	23

Coordinates and Z score refer to the peak of each brain region. BA = Brodmann area; L = left; R = right; LG = lingual gyrus; FG = fusiform gyrus; MFG = medial frontal gyrus; SFG = superior frontal gyrus; MTG = middle temporal gyrus; STG = superior temporal gyrus; IFG = inferior frontal gyrus; MPFC = medial prefrontal cortex; STS = superior temporal sulcus; OFC = orbitofrontal cortex.

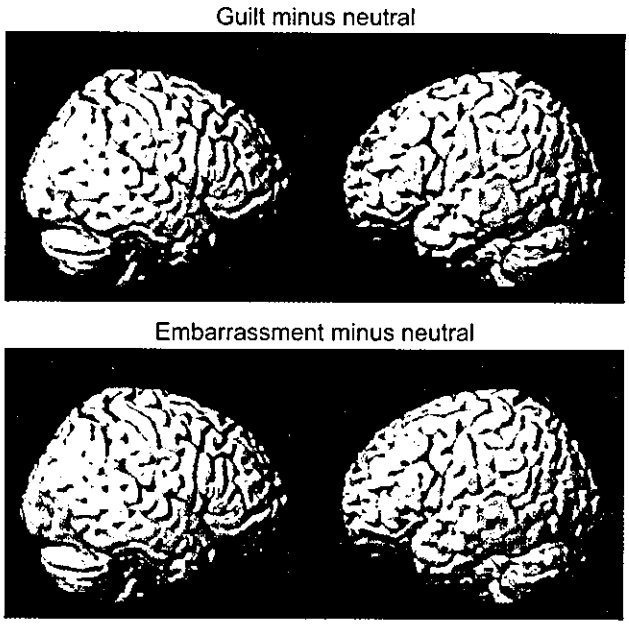

Fig. 2. Images showing brain activation in guilt and embarrassment conditions relative to neutral condition. Guilt minus neutral (top). Activated regions were in the MPFC, posterior STS, and visual cortex. Embarrassment minus neutral (bottom). In addition to activations in the MPFC, left posterior STS, and visual cortex, more widespread activations were shown in the left OFC, left temporal cortex (anterior and middle), and right temporal cortex (anterior). Note that both emotional conditions commonly activated the MPFC, left posterior STS, and visual cortex. Significant differences were recognized at a height threshold ($Z > 3.09$; $P < 0.001$, uncorrected) and extent threshold (15 voxels).

0.001, uncorrected) and extent threshold (15 voxels). We used a relatively large extent threshold to sufficiently minimize the risk of type 1 errors due to the relatively low height threshold. To assess common areas activated by the guilt and embarrassment conditions, we created a mask from the G − N contrast in the random effect analysis (threshold at $P < 0.001$, uncorrected). This mask was applied inclusively to the E − N contrast.

To ensure relative differences between activity associated with guilt and embarrassment, random effect analyses of guilt minus embarrassment contrast (G − E) and embarrassment minus guilt contrast (E − G) were conducted. Because one of the aims of this study was to investigate differences between guilt and embarrassment at the neural basis level, we reported the differences at a lower threshold (height threshold at $P < 0.005$, uncorrected, and extent threshold of 15 voxels).

We conducted additional analysis to demonstrate a more direct link between regional brain activity with subjective emotional judgments. Using the mean of ratings of guilt and embarrassment for each subject as the covariate, regression analyses with the contrast (G − N and E − N) and the covariate were done at the second level (height threshold at $P < 0.001$, uncorrected, and extent threshold of 15 voxels). Using the effect sizes, representing the percent signal change, of the contrasts (E − N and G − N) at the peak coordinates uncovered by regression analyses, we plotted fMRI signal changes and ratings of guilt and embarrassment. Coordinates of activation were converted from MNI coordinates to the Talairach and Tournoux (1988) coordinates using the mni2tal algorithm (M. Brett, Cambridge, MA).

Results

Self-rating

The neutral sentences were judged as carrying neither guilty nor embarrassing contents. The mean ratings of guilt and embarrassment for neutral sentences were, respectively, 1.0 (SD = 0.0) and 1.0 (SD = 0.0), for guilt-related sentences 4.1 (SD = 0.7) and 1.6 (SD = 0.7), and for embarrassing sentences 1.5 (SD = 0.4) and 3.7 (SD = 0.6). The mean ratings of guilt were significantly greater for guilt-related sentences than for embarrassing sentences ($t = 10.6$, $df = 36$, $P < 0.001$). The mean ratings of embarrassment were significantly greater for embarrassing sentences than for guilt-related sentences ($t = 12.4$, $df = 36$, $P < 0.001$).

fMRI result

Guilt condition relative to neutral condition (G − N) produced greater activations in the MPFC, left posterior STS, and visual cortex. Embarrassment condition relative to neutral condition (E − N) produced greater activations in the MPFC, left posterior STS, left temporal cortex (anterior and middle), left orbitofrontal cortex (OFC), right temporal cortex (anterior), left hippocampus, and visual cortex (Table 2 and Fig. 2). In other words, both conditions commonly activated the MPFC, left posterior STS, and visual cortex (Table 3), but the embarrassment condition produced more widespread activations in the left temporal cortex (anterior and middle), right temporal cortex (anterior), left OFC, and left hippocampus.

Embarrassment condition relative to guilt condition (E − G) produced greater activation in the right temporal cortex (anterior), bilateral hippocampus, and visual cortex. In contrast, guilt condition relative to embarrassment condition (G − E) produced greater activation in the MPFC (Table 4 and Fig. 3).

Regression analyses revealed positive linear correlations between self-rating of guilt and the degree of activation in the

Table 3
Brain regions commonly activated by guilt and embarrassment conditions

Brain region	Coordinates			BA	Z score	Voxels
	x	y	z			
L visual cortex (LG)	−12	−77	6	17,18,19	4.37	1021
R visual cortex (LG)	2	−85	6	17,18	5.41	
L MPFC (MFG, SFG)	−10	36	52	8,9,10	4.35	429
R MPFC (MFG)	4	57	16	10	3.62	
L posterior STS (MTG)	−44	−61	20	39	4.4	101

A mask from the G − N contrast by random effect analysis (threshold at $P < 0.001$, uncorrected) was applied inclusively to the E − N contrast (height threshold at $P < 0.001$, uncorrected, and extent threshold of 15 voxels). See Table 2 legend.

Table 4
Comparisons between regional brain activities associated with guilt and embarrassment

Brain region	Coordinates			BA	Z score	Voxels
	x	y	z			
Embarrassment minus guilt						
R visual cortex (cuneus, LG, FG)	12	−83	8	17,18,19	3.28	393
R visual cortex (IOG)	38	−68	−5	19	3.59	49
L visual cortex (LG)	−10	−62	−2	18,19	3.48	140
L visual cortex (LG)	−8	−80	1	19	2.86	77
R anterior temporal cortex (MTG)	42	−3	−27	21	2.96	25
R hippocampus	32	−18	−13		2.91	32
L hippocampus	−20	−14	−9		3.21	49
Guilt minus embarrassment						
L MPFC (MFG)	−16	49	14	10	3.39	24

Random effect analyses of G − E and E − G contrast were conducted. See Table 2 legend.

MPFC (medial frontal gyrus, $x = -8$, $y = 55$, $z = 3$; $Z = 4.26$; 31 voxels), posterior STS (middle temporal gyrus, $x = -58$, $y = -56$, $z = 10$; $Z = 4.23$; 81 voxels), and visual cortex (lingual gyrus, $x = -14$, $y = -58$, $z = 3$; $Z = 3.82$; 24 voxels). There were positive linear correlations between self-rating of embarrassment and the degree of activation in the posterior STS (middle temporal gyrus, $x = -46$, $y = -57$, $z = 23$; $Z = 3.88$; 37 voxels) and visual cortex (lingual gyrus, $x = -16$, $y = -49$, $z = -4$; $Z = 3.48$; 20 voxels) (Figs. 4 and 5).

Discussion

We investigated the neural response associated with evaluative processes of self-conscious moral emotions. Recent neuroimaging studies have reported the neural substrate of moral judgment (Greene et al., 2001; Moll et al., 2002a,b). However, few reports are available on specific moral or social emotions (Berthoz et al., 2002; Shin et al., 2000). This study showed similarities and differences during evaluative processes of two moral emotions, guilt and embarrassment, at the neural basis level by measurements of neural responses in the same session.

As we predicted, both guilt and embarrassment conditions relative to neutral condition commonly produced greater activity in the components of neural substrates of social cognition or ToM, the MPFC, left posterior STS, along with the visual cortex. Several neuroimaging studies in healthy subjects using different variants of the ToM paradigm have consistently reported activation in the MPFC, predominantly on the left side (Fletcher et al., 1995; Gallagher et al., 2000; Goel et al., 1995). Additionally, autism, which is considered to have impairments in ToM, showed reduced activation in the MPFC (Baron-Cohen et al., 1999; Castelli et al., 2002; Happe et al., 1996). The MPFC has been suggested to play an important role in monitoring one's own mental state as well as that of others (Castelli et al., 2000; Frith, 2001). Recent studies reported that the MPFC was also recruited in moral judgment (Greene et al., 2001; Heekeren et al., 2003).

Activations in the posterior STS have also been consistently reported in social cognition or ToM tasks (Calder et al., 2002; Castelli et al., 2000; Gallagher et al., 2000; Winston et al., 2002) and in moral judgment tasks (Greene et al., 2001; Heekeren et al., 2003), while the area identical to the posterior STS was variously described as the temporoparietal junction or angular gyrus. Originally, STS was known to be activated by biological motions such as movement of eyes, mouth, hands, and body, but it has been suggested to have a more general function in social cognition (Adolphs, 2001; Allison et al., 2000), detection of intention (Gallagher et al., 2000), evaluation of trustworthiness of faces (Winston et al., 2002), detection of the behavior of agents and analysis of goal, and outcome of the behavior (Frith, 2001; Frith and Frith, 1999).

Common activations in the MPFC and posterior STS support the notion that both guilt and embarrassment are self-conscious

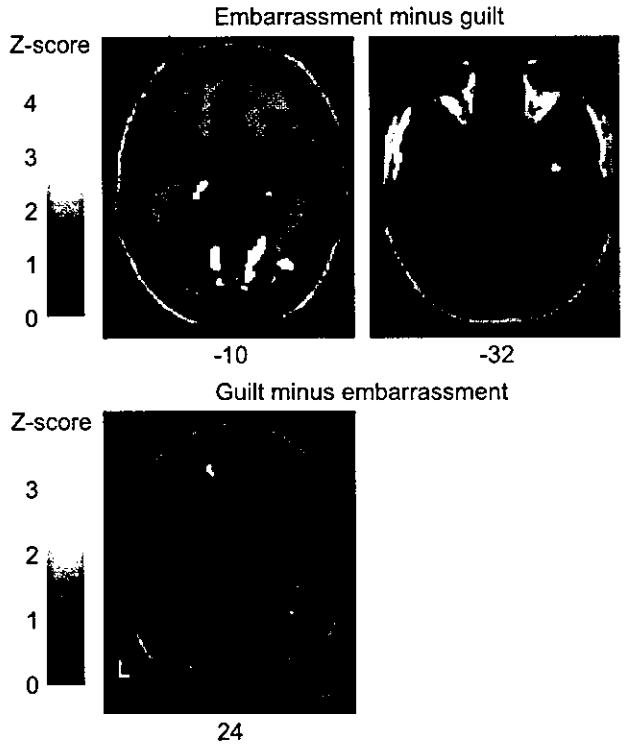

Fig. 3. Comparison of guilt and embarrassment conditions with height threshold ($P < 0.005$) and extent threshold (15 voxels). Embarrassment minus guilt (top). Compared to guilt, greater activation was shown in the right temporal cortex (anterior), bilateral hippocampus, and visual cortex. Guilt minus embarrassment (bottom). Compared to embarrassment, greater activation was shown in the MPFC. The bar shows the range of the Z score. Within the image, L indicates left. Numbers in the bottom row indicate the z coordinates of the Montreal Neurological Institute brain.

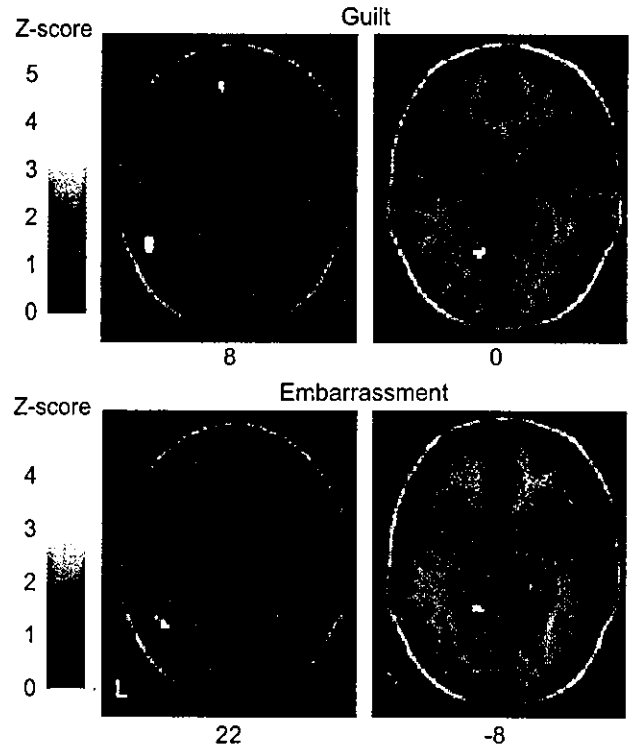

Fig. 4. Correlation between brain activation and the self-ratings of guilt and embarrassment with height threshold ($P < 0.005$) and extent threshold (15 voxels). There were positive linear correlations between self-rating of guilt and the degree of activation in the posterior STS and visual cortex (top). There were positive linear correlations between self-rating of embarrassment and the degree of activation in the posterior STS and visual cortex (bottom). The bar shows the range of the Z score. Within the image, L indicates left. Numbers in the bottom row indicate the z coordinates of the Montreal Neurological Institute brain.

emotions that can arise from concerns about others' evaluation of one's own behavior (Eisenberg, 2000; Haidt, 2003; Tangney and Dearing, 2002). In other words, one needs the ability to take the perspective of others and to represent their mental state, that is, ToM, to understand the sense of guilt or embarrassment.

In spite of our attempt to control the linguistic features of the visual stimuli, increased activations were found in the visual cortex in response to the emotional conditions relative to the neutral condition. Enhanced visual cortex activations by emotionally salient visual stimuli have been extensively reported (Phan et al., 2002; Takahashi et al., 2004). Emotionally salient stimuli or attention demanding stimuli have been suggested as modulating sensory processing in the visual cortex. Early visual cortex receives prominent feedback projection from limbic structures such as amygdala (Emery and Amaral, 2000), and such pathway could act to enhance visual processing (Morris et al., 1998; Vuilleumier et al., 2001).

Interestingly, compared to the G – N contrast, the E – N contrast demonstrated more widespread activations in the left temporal cortex (anterior and middle), right temporal cortex (anterior), left OFC, and left hippocampus. Direct comparison between guilt and embarrassment conditions showed that the E – G contrast demonstrated significantly greater activation in the right anterior temporal cortex, bilateral hippocampus, and visual cortex. All these regions are also considered as the brain area related to social or moral cognition (Adolphs, 2001; Casebeer, 2003; Greene and Haidt, 2002; Moll et al., 2003). We did not expect the greater activation in the hippocampus in the embarrassment condition. The hippocampus is suggested to engage in retrieving behaviorally relevant memories (Strange et al., 1999). In moral judgment, the hippocampus might facilitate conscious recollection of memories that allow past events to affect current decisions (Casebeer, 2003).

Embarrassment has a higher affinity to the violation of social conventions (choices of clothing, etiquette and hygiene, etc.) that depend on societies or cultures, while guilt has a higher affinity to the violation of moral norms (issues of harm, right and justice, etc.) that are universal among human beings (Eisenberg, 2000; Haidt, 2003; Tangney et al., 1996). Moreover, embarrassment is uniquely a public emotion that depends on a real or imagined presence of others among one's self-conscious emotions. If people do experience embarrassment in private, it is a situation of vividly imagining what others might think of them (Miller, 1996; Tangney et al., 1996). Guilt does not necessarily depend on personal acquaintances. Guilt could be elicited not only by concerns with others' evaluation of self but also by private conscience (Haidt, 2003; Tangney and Dearing, 2002; Tangney et al., 1996). In light of these points, embarrassment could be regarded as a more social and public emotion that depends on personal interactions. Regression analyses showed that subjective ratings of guilt and embarrassment correlated with the degree of activation in the posterior STS, visual cortex, and MPFC, brain areas commonly activated by both emotional conditions. In other words, emotional intensity did not appear to account for the more widespread activation observed in embarrassment condition. Considering the regression analyses results, our interpretation was that the additional activations found in embarrassment condition might reflect more complex processes that detect and understand the complex social information of embarrassment.

This study has some limitations. First, a moral emotion could be accompanied by another emotion. For instance, guilt and shame could co-occur in some situations (Eisenberg, 2000). In moral transgression, people may feel guilty for violating a social norm and at the same time might feel shameful about one's own shortcomings. For this reason, we carefully chose the situations, although we understand that it is not feasible to extract "pure" emotion. Second, as mentioned above, embarrassment depends on society and culture. The social background of participants, such as gender, generation, religion, and education, could be confounding factors. Further studies that can control these factors would be recommended. Finally, we should acknowledge general limitations of a functional imaging study to reveal the neural substrates of social cognition or social emotions. The processing of social information is distributed in space and time, ranging from the perception of socially relevant stimuli to the elicitation of social behavior. Most functional imaging studies focused on the perception and interpretation of socially relevant stimuli. Emotional judgment tasks such as facial expression discrimination task or our task could also be regarded as a task of the perception and interpretation of socially relevant stimuli. It should be noted that emotional states that elicit social or emotional behaviors are not necessarily induced by merely viewing facial expressions or reading sentences. Social cognition is a domain with fuzzy boundaries and vaguely specified components. Processes of social cognition overlap with those of emotions. Although it is difficult to assess specific components of social cognition or emotions by a single modality, at least in this study, we assessed the evaluative processes of moral emotions. To complement fMRI studies, electrophysiological methods that have good temporal resolution

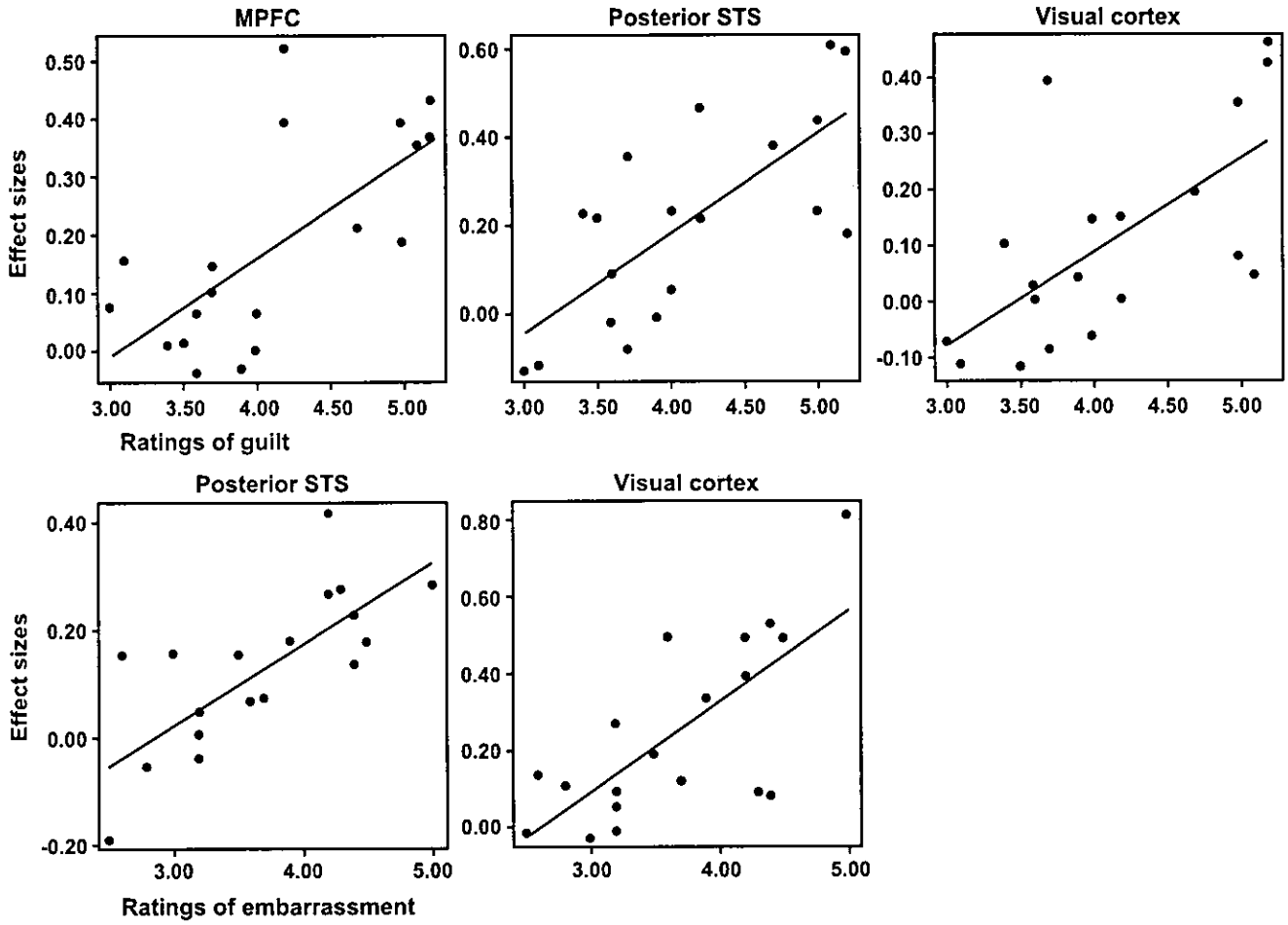

Fig. 5. Plots and regression lines of correlations between self-ratings and degree of activation in the brain regions. There were correlations between self-rating of guilt and degree of activation in the MPFC ($x = -8, y = 55, z = 3, r = 0.686, P < 0.005$), posterior STS ($x = -58, y = -56, z = 10, r = 0.722, P < 0.005$), and visual cortex ($x = -14, y = -58, z = 3, r = 0.653, P < 0.005$) (top). There were positive linear correlations between self-rating of embarrassment and degree of activation in the posterior STS ($x = -46, y = -57, z = 23, r = 0.744, P < 0.005$) and visual cortex ($x = -16, y = -49, z = -4, r = 0.719, P < 0.005$) (bottom).

would be recommended. Moreover, it is difficult to assess real-life human social behavior or to induce complex emotions in an MRI environment. Lesion studies can at least indicate the structures necessary for mediating social behavior (Adolphs, 2003).

Notwithstanding the difficulties in measuring social behavior, recording autonomic responses will be useful for assessing some aspects of social behavior or emotional responses. For instance, monitoring blushing, the hallmark of embarrassment, by recording face temperature or facial blood flow will be useful to distinguish embarrassment from guilt (Gerlach et al., 2003).

In conclusion, we investigated the neural substrates of evaluative processes of specific moral emotions and demonstrated similarities and differences between guilt and embarrassment at the neural basis level. Supporting the concept that both guilt and embarrassment could be regarded as self-conscious emotions, both emotional conditions produced similar activation patterns in the components of neural substrates implicated in social cognition or ToM. Moreover, our fMRI data lead us to conjecture that the evaluative process of embarrassment might be a more complex process than that of guilt. We expect our findings to contribute to a broadening of the knowledge concerning the neural basis of amoral behavior observed in neurological and psychiatric disorders.

Acknowledgments

We thank Professor Toru Nishikawa of the Section of Psychiatry and Behavioral Science, Graduate School of Medicine, Tokyo Medical and Dental University. The staff of the Section of Biofunctional Informatics, Graduate School of Medicine, Tokyo Medical and Dental University, and of Asai Hospital are gratefully acknowledged. This work was supported by a Grant-in-Aid for Scientific Research from the Japanese Ministry of Education, Culture, Sports, Science and Technology (15390348), a research grant for nervous and mental disorders (14B-3), and a Health and Labor Sciences Research Grant for Research on Psychiatric and Neurological Diseases and Mental Health (H15-KOKORO-003) from the Japanese Ministry of Health, Labor and Welfare.

References

Adolphs, R., 2001. The neurobiology of social cognition. Curr. Opin. Neurobiol. 11, 231–239.

Adolphs, R., 2003. Investigating the cognitive neuroscience of social behavior. Neuropsychologia 41, 119–126.

Allison, T., Puce, A., McCarthy, G., 2000. Social perception from visual cues: role of the STS region. Trends Cogn. Sci. 4, 267–278.

Anderson, S.W., Bechara, A., Damasio, H., Tranel, D., Damasio, A.R., 1999. Impairment of social and moral behavior related to early damage in human prefrontal cortex. Nat. Neurosci. 2, 1032–1037.

Baron-Cohen, S., Ring, H.A., Wheelwright, S., Bullmore, E.T., Brammer, M.J., Simmons, A., Williams, S.C., 1999. Social intelligence in the normal and autistic brain: an fMRI study. Eur. J. Neurosci. 11, 1891–1898.

Beer, J.S., Heerey, E.A., Keltner, D., Scabini, D., Knight, R.T., 2003. The regulatory function of self-conscious emotion: insights from patients with orbitofrontal damage. J. Pers. Soc. Psychol. 85, 594–604.

Berthoz, S., Armony, J.L., Blair, R.J., Dolan, R.J., 2002. An fMRI study of intentional and unintentional (embarrassing) violations of social norms. Brain 125, 1696–1708.

Brower, M.C., Price, B.H., 2001. Neuropsychiatry of frontal lobe dysfunction in violent and criminal behaviour: a critical review. J. Neurol., Neurosurg. Psychiatry 71, 720–726.

Calder, A.J., Lawrence, A.D., Keane, J., Scott, S.K., Owen, A.M., Christoffels, I., Young, A.W., 2002. Reading the mind from eye gaze. Neuropsychologia 40, 1129–1138.

Capps, L., Yirmiya, N., Sigman, M., 1992. Understanding of simple and complex emotions in non-retarded children with autism. J. Child Psychol. Psychiatry 33, 1169–1182.

Casebeer, W.D., 2003. Moral cognition and its neural constituents. Nat. Rev., Neurosci. 4, 840–846.

Castelli, F., Happe, F., Frith, U., Frith, C.D., 2000. Movement and mind: a functional imaging study of perception and interpretation of complex intentional movement patterns. NeuroImage 12, 314–325.

Castelli, F., Frith, C.D., Happe, F., Frith, U., 2002. Autism, Asperger syndrome and brain mechanisms for the attribution of mental states to animated shapes. Brain 125, 1839–1849.

Eisenberg, N., 2000. Emotion, regulation, and moral development. Annu. Rev. Psychol. 51, 665–697.

Emery, N.J., Amaral, D.G., 2000. The role of the amygdala in primate social cognition. In: Lane, R.D., Nadel, L. (Eds.), Cognitive Neuroscience of Emotion. Oxford Univ. Press, New York, pp. 156–191.

Fletcher, P.C., Happe, F., Frith, U., Baker, S.C., Dolan, R.J., Frackowiak, R.S., Frith, C.D., 1995. Other minds in the brain: a functional imaging study of "theory of mind" in story comprehension. Cognition 57, 109–128.

Frith, U., 2001. Mind blindness and the brain in autism. Neuron 32, 969–979.

Frith, C.D., Frith, U., 1999. Interacting minds—A biological basis. Science 286, 1692–1695.

Gallagher, H.L., Happe, F., Brunswick, N., Fletcher, P.C., Frith, U., Frith, C.D., 2000. Reading the mind in cartoons and stories: an fMRI study of 'theory of mind' in verbal and nonverbal tasks. Neuropsychologia 38, 11–21.

Gerlach, A.L., Wilhelm, F.H., Roth, W.T., 2003. Embarrassment and social phobia: the role of parasympathetic activation. J. Anxiety Disord. 17, 197–210.

Goel, V., Grafman, J., Sadato, N., Hallett, M., 1995. Modeling other minds. NeuroReport 6, 1741–1746.

Greene, J.D., Haidt, J., 2002. How (and where) does moral judgment work? Trends Cogn. Sci. 6, 517–523.

Greene, J.D., Sommerville, R.B., Nystrom, L.E., Darley, J.M., Cohen, J.D., 2001. An fMRI investigation of emotional engagement in moral judgment. Science 293, 2105–2108.

Haidt, J., 2003. The moral emotions. In: Davidson, R.J., Scherer, K.R., Goldsmith, H.H. (Eds.), Handbook of Affective Sciences. Oxford Univ. Press, Oxford, pp. 852–870.

Happe, F., Ehlers, S., Fletcher, P., Frith, U., Johansson, M., Gillberg, C., Dolan, R., Frackowiak, R., Frith, C., 1996. 'Theory of mind' in the brain. Evidence from a PET scan study of Asperger syndrome. NeuroReport 8, 197–201.

Heekeren, H.R., Wartenburger, I., Schmidt, H., Schwintowski, H.P., Villringer, A., 2003. An fMRI study of simple ethical decision-making. NeuroReport 14, 1215–1219.

Heerey, E.A., Keltner, D., Capps, L.M., 2003. Making sense of self-conscious emotion: linking theory of mind and emotion in children with autism. Emotion 3, 394–400.

Hillier, A., Allinson, L., 2002. Understanding embarrassment among those with autism: breaking down the complex emotion of embarrassment among those with autism. J. Autism Dev. Disord. 32, 583–592.

Keltner, D., Buswell, B.N., 1997. Embarrassment: its distinct form and appeasement functions. Psychol. Bull. 122, 250–270.

Lewis, M., 1993. Self-conscious emotions: embarrassment, pride, shame and guilt. In: Lewis, M., Haviland, J.M. (Eds.), Handbook of Emotions. Guilford Press, New York, pp. 623–636.

Miller, R.S., 1996. Embarrassment: Poise and Peril in Everyday Life. Guilford Press, New York.

Miller, B.L., Diehl, J., Freedman, M., Kertesz, A., Mendez, M., Rascovsky, K., 2003. International approaches to frontotemporal dementia diagnosis: from social cognition to neuropsychology. Ann. Neurol. 54, S7–S10.

Moll, J., de Oliveira-Souza, R., Bramati, I.E., Grafman, J., 2002a. Functional networks in emotional moral and nonmoral social judgments. NeuroImage 16, 696–703.

Moll, J., de Oliveira-Souza, R., Eslinger, P.J., Bramati, I.E., Mourao-Miranda, J., Andreiuolo, P.A., Pessoa, L., 2002b. The neural correlates of moral sensitivity: a functional magnetic resonance imaging investigation of basic and moral emotions. J. Neurosci. 22, 2730–2736.

Moll, J., de Oliveira-Souza, R., Eslinger, P.J., 2003. Morals and the human brain: a working model. NeuroReport 14, 299–305.

Morris, J.S., Friston, K.J., Buchel, C., Frith, C.D., Young, A.W., Calder, A.J., Dolan, R.J., 1998. A neuromodulatory role for the human amygdala in processing emotional facial expressions. Brain 121, 47–57.

Phan, K.L., Wager, T., Taylor, S.F., Liberzon, I., 2002. Functional neuroanatomy of emotion: a meta-analysis of emotion activation studies in PET and fMRI. NeuroImage 16, 331–348.

Pinkham, A.E., Penn, D.L., Perkins, D.O., Lieberman, J., 2003. Implications for the neural basis of social cognition for the study of schizophrenia. Am. J. Psychiatry 160, 815–824.

Shin, L.M., Dougherty, D.D., Orr, S.P., Pitman, R.K., Lasko, M., Macklin, M.L., Alpert, N.M., Fischman, A.J., Rauch, S.L., 2000. Activation of anterior paralimbic structures during guilt-related script-driven imagery. Biol. Psychiatry 48, 43–50.

Snowden, J.S., Neary, D., Mann, D.M., 2002. Frontotemporal dementia. Br. J. Psychiatry 180, 140–143.

Strange, B.A., Fletcher, P.A., Henson, R.N.A., Friston, K.J., Dolan, R.J., 1999. Segregating the functions of human hippocampus. Proc. Natl. Acad. Sci. U. S. A. 96, 4034–4039.

Takahashi, H., Koeda, M., Oda, K., Matsuda, T., Matsushima, E., Matsuura, M., Asai, K., Okubo, Y., 2004. An fMRI study of differential neural response to affective pictures in schizophrenia. NeuroImage 22, 1247–1254.

Talairach, J., Tournoux, P., 1988. Co-Planar Stereotaxic Atlas of the Human Brain: Three-Dimensional Proportional System. Thieme Medical, New York.

Tangney, J.P., Dearing, R.L., 2002. Shame and Guilt. Guilford Press, New York.

Tangney, J.P., Miller, R.S., Flicker, L., Barlow, D.H., 1996. Are shame, guilt, and embarrassment distinct emotions? J. Pers. Soc. Psychol. 70, 1256–1269.

Vuilleumier, P., Armony, J.L., Driver, J., Dolan, R.J., 2001. Effects of attention and emotion on face processing in the human brain: an event-related fMRI study. Neuron 30, 829–841.

Winston, J.S., Strange, B.A., O'Doherty, J., Dolan, R.J., 2002. Automatic and intentional brain responses during evaluation of trustworthiness of faces. Nat. Neurosci. 5, 277–283.

—Photogravure—

Pharmacological Modulations on the Human Cognitive Processes: An fMRI Study

Noriaki Yahata[1], Hidehiko Takahashi[2] and Yoshiro Okubo[1]
[1]Department of Neuropsychiatry, Nippon Medical School
[2]Asai Hospital

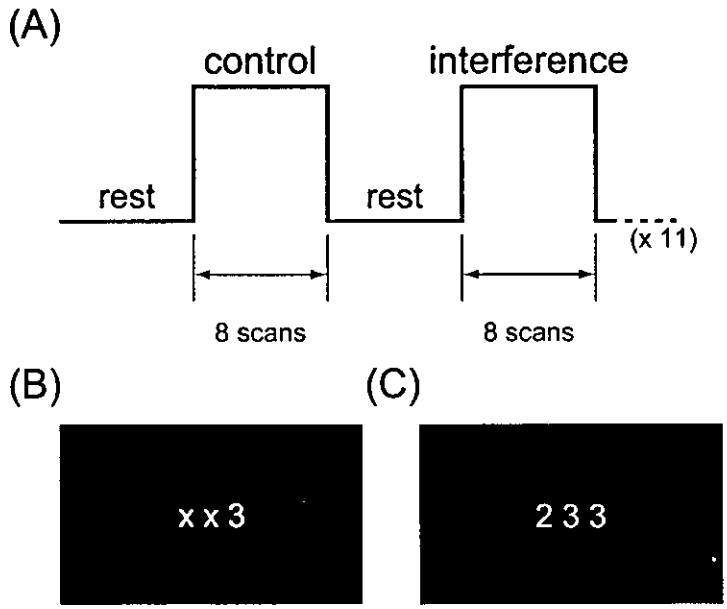

Fig. 1

Investigating modulatory effects of psychopharmacological agents in the human brain allows for not only functional characterization of particular neurotransmitter systems in the human cognition, but better understanding of pathophysiology and treatment of neuropsychiatric disorders[1]. Here we conducted a functional magnetic resonance imaging (fMRI) study to map effects of a dopamine D_2 antagonist (sultopride) on a decision-making process. In a single scanning session, ten male, right-handed, healthy subjects performed a Stroop-like cognitive interference task[2] (**Fig. 1**). In the absence of dopaminergic manipulations, comparison of blood oxygenation level dependent (BOLD) signals during the interference condition against those during the control condition revealed a widely distributed network implicated in the decision-making process with cognitive interference (**Fig. 2A**). Upon the administration of the D_2 antagonist, however, many of these regions exhibited decreased activities, and the effects were found to be most prominent in regions around the cerebellum, the thalamus, the anterior cingulate cortex, and the motor areas (**Fig. 2B**). Subsequent studies should address the role of individual components in the observed brain circuits, as well as what the decrements of activations mean in the neurophysiological context.

Correspondence to Noriaki Yahata, Department of Neuropsychiatry, Nippon Medical School, 1-1-5 Sendagi, Bunkyo-ku, Tokyo 113-8603, Japan
E-mail: yahata@nms.ac.jp
Journal Website (http://www.nms.ac.jp/jnms/)

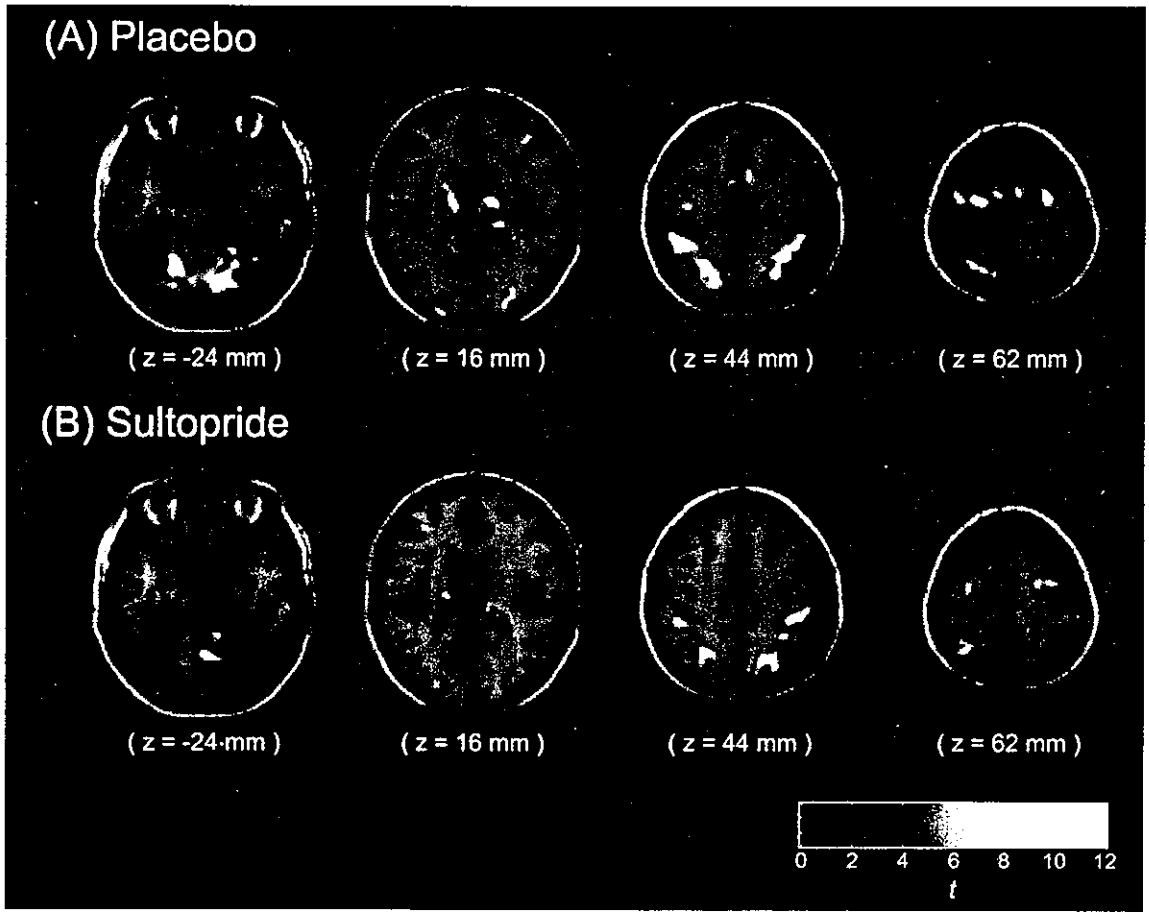

Fig. 2

Fig. 1 (A) Schematic diagram illustrating the cognitive interference task employed. A single scanning session consisted of blocks (containing eight scans) of control and interference trials interspaced by resting periods. During the trials, subjects are instructed to report by button press the identity of the number that differs from the other two. (B)-(C) Examples of the trials. During the control trials, the distractors were the letter 'x', whereas during the interference trials, the distractors were other numbers, thereby imposing higher cognitive demands.

Fig. 2 Activated regions during the interference trials in contrast to the control trials (A) with no dopaminergic manipulations and (B) under the administration of a D_2 antagonist (sultopride). The results are based on a group analysis with statistical parametric mapping (SPM) software[3] and with a statistical threshold of $P < 0.001$ (uncorrected).

References

1. Honey G, Bullmore E: Human pharmacological MRI. Trends Pharmacol Sci 2004; 25: 366–374.
2. Bush G, Shin LM, Holmes J, Rosen BR, Vogt BA: The Multi-Source Interference Task: validation study with fMRI in individual subjects. Mol Psychiatry 2003; 8: 60–70.
3. Friston KJ, Holmes AP, Worsley KJ, Poline JP, Frith CD, Frackowiak RSJ: Statistical parametric maps in functional imaging: A general linear approach. Hum Brain Mapp 1995; 2: 189–210.

Original Paper

Cerebrovascular Diseases

Cerebrovasc Dis 2004;18:22–29
DOI: 10.1159/000078604

Received: July 23, 2003
Accepted: January 6, 2004
Published online: May 19, 2004

Long-Term Change in Size of Cerebral Infarction: Predictive Value of Brain Perfusion SPECT Using Statistical Parametric Mapping

Hiroshige Watanabe[a] Yuji Murata[a] Isamu Ohashi[a] Kenji Oda[b]
Eisuke Matsushima[b] Yoshiro Okubo[b] Hitoshi Shibuya[a]

Departments of [a]Radiology and [b]Psychiatry, Faculty of Medicine, Tokyo Medical and Dental University, Tokyo, Japan

Key Words
Brain infarction · Brain ischemia · Brain MR · Single photon emission computed tomography

Abstract
A focus of infarction is surrounded by hypoperfused areas. The present study was undertaken to examine the long-term changes in the size of infarcts, the relationship between the size of an infarct and the extent of the surrounding hypoperfused areas, and the background of such changes. The subjects of this study were 11 patients with ischemic lesions of the brain who had undergone brain SPECT (^{99m}Tc-ethyl cysteinate dimer) within 1 week after initial MRI, and who underwent MRI again more than half a year later. Statistical parametric mapping (SPM) was conducted to detect significantly hypoperfused areas on the SPECT images. Relative size of significantly hypoperfused areas on SPM and infarcts on T_2-weighted MR images were measured. The patients were divided into two groups based on the percentage of the infarct's size relative to the size of the surrounding hypoperfused areas (75–125 and 0–39%). Infarcts in the '75–125%' group showed little change in size, while in the '0–39%' group infarcts increased slowly until it reached the same rate as the former group. All patients with infarct in the '0–39%' group were noted to have severe stenosis of the internal carotid arteries bilaterally. Patients having severe stenosis of the internal carotid artery often had a slowly enlarging infarct. SPM seems to be useful in predicting the ultimate size of the infarct.

Introduction

In regard to the size of cerebral infarcts, it has been reported that many infarcts reach their peak volume within 3 days (more significantly within the first 24–36 h) after the onset, and that their size starts to decrease till the 7th day, to reach their ultimate size [1–3]. It is thought that the most important pathophysiological changes in stroke take place during the first few days after the symptom onset [4].

An infarct is usually surrounded by an area of hypoperfused tissue [5]. The size of the hypoperfused area around an infarct differs from case to case, but the volume of this area is relatively large during the acute stage of infarction, and this area may be deemed as a reversibly ischemic area [6, 7]. It has been suggested that treatment or reperfusion during the acute stage may prevent progression of the extent of infarction and thus improve the prognosis of the patient. Prompted by this suggestion, a number of studies have been conducted, focusing on the acute stage of infarction [8–11].

KARGER
Fax + 41 61 306 12 34
E-Mail karger@karger.ch
www.karger.com

1015–9770/04/0181–0022$21.00/0

Accessible online at:
www.karger.com/ced

Hiroshige Watanabe, MD
Department of Radiology, Faculty of Medicine
Tokyo Medical and Dental University, 5-45, 1-chome, Yushima, Bunkyo-ku
Tokyo 113-8519 (Japan)
Tel. +81 3 5803 5311, Fax +81 3 5803 0147, E-Mail wat@aw.catv.ne.jp

Table 1. Cerebrovascular lesions, the time and findings of/from diagnostic imaging, and treatment in each patient

Patient No.	Age	Sex	Site of cerebrovascular lesion	Infarct No.	Site of infarct	From onset to MRI[1]	From MRI to SPECT[2]	Treatment
1	23	F	Moyamoya disease, bilateral ICA stenosis (+) (bil. stage IIIc)	1	Lt. MCA perfusion territory	18	4	Bilateral EDAS (77 days) Aspirin therapy
2	68	M	Lt. ICA stenosis (95%), Rt. ICA stenosis (70%)	2a	Lt. MCA perfusion territory	7	4	Urokinase therapy (0 days)
				2b	Lt. occipital pole	Unknown		Heparin → warfarin therapy
				2c	Rt. external capsule	Unknown		Lt. carotid endarterectomy (102 days)
				2d	Rt. putamen	Unknown		
				2e	Lt. middle temporal gyrus	Unknow		
3	72	F	Rt. ICA occlusion, Lt. ICA stenosis (75%)	3a	Rt. mid-brain	1	3	Anticoagulation therapy → warfarin therapy
				3b	Rt. basal ganglia	1		
4	4	M	Moyamoya disease (bil. stage IIIb)	4	Lt. anterolateral angle	1	0	Bil. EDAS (8 days)
5	1	F	Moyamoya disease, bilateral ICA occlusion (+)	5a	Lt. PCA perfusion territory	1	0	Warfarin therapy
				5b	Rt. MCA perfusion territory	24		(post-bil. EDAS)
6	79	M	Lt. PCA stenosis	6a	Lt. thalamus	1	5	Urokinase therapy (0 days)
				6b	Rt. putamen	Unknown		Antiplatelet therapy
				6c	Lt. putamen	Unknown		
7	12	F	Moyamoya disease, bilateral ICA stenosis (+)	7a	Lt. middle frontal gyrus	8	2	Aspirin therapy
			(Rt. stage II, Lt. stage II–IIIa)	7b	Rt. superior frontal gyrus	44		Rt. EDAS (60 days)
8	52	M		8	Lt. posterior parietal artery	2	7	Aspirin therapy
9	61	F	Lt. MI occlusion, Rt. IC aneurysm	9	Lt. middle temporal gyrus	581	2	
10	52	F	Lt. MCA occlusion	10	Lt. semoval center	74	0	
11	45	F	Moyamoya disease (Lt. EDAS) Lt. MCA occlusion, Rt. ACA occlusion Rt. MCA stenosis	11	Lt. middle temporal gyrus	984	0	

[1] Days from the episode of stroke symptom which caused the infarct to initial MRI in this study.
[2] Days from initial MRI to SPECT.

Is it correct to say that the size of an infarct is determined during the acute stage in most cases, and that it does not change thereafter? It is known that some infarcts show a tendency towards extension even after the acute stage [2]. To our knowledge, however, no report has been published concerning the long-term changes in the sizes of infarcts during the subacute to chronic stages.

The present study was undertaken to examine the long-term changes in the sizes of infarcts, the relationship between the sizes of infarcts and the extent of the surrounding hypoperfused areas, and the background of such changes.

Patients, Materials and Methods

Of all the patients who underwent MRI at the Department of Radiology of our hospital for detailed evaluation following the occurrence of cerebral ischemic stroke between January 1998 and May 2001, those who had infarcts and underwent cerebral angiography were selected for this study. Eleven patients (4 males and 7 females, age range 1–72 years, mean age 42.6 years) with a total of 20 foci of infarcts were registered for this study (table 1). All these 11 patients underwent brain SPECT (^{99m}Tc-ethyl cysteinate dimer) within 1 week after initial MRI, and underwent MRI again more than half a year later. The following patients were excluded from the evaluation: 1 patient who developed another focus of infarct in the vicinity of the first one during the follow-up period, and 4 patients with small infarcts (≤10 mm) in the deep white matter that could not be detected by SPECT.

For each patient, the cerebral angiogram images obtained after the attack were analyzed to check for underlying cerebrovascular lesions. Of the 11 patients, 7 were found to have severe stenotic lesions of the internal carotid arteries bilaterally. Of the remaining 4 patients, 2 had MCA occlusion, 1 had stenosis of the PCA, and 1 had no cerebrovascular lesions.

MR Imaging

In the present study, MRI was used for the detection of infarcts. MR images were obtained using a 1.5-Tesla system (Magnetom Vision, Siemens Medical Systems, Erlangen, Germany; Signa, General Electric Medical Systems, Milwaukee, Wisc., USA). The size of the infarct was determined from transverse T_2-weighted MR images (repetition time 4,000 ms; echo time 96.2 ms; matrix size 256 × 256; field of view 200 mm; section thickness of 4 mm with an intersection gap of 0.4 mm).

SPECT Scanning

SPECT was used to detect hypoperfused tissue around the infarct core, using ^{99m}Tc-ethyl cysteinate dimer as the tracer; 800 MBq of the tracer was injected into the right cubital vein of the patient lying in the supine position.

Fifteen minutes after the injection, SPECT imaging was performed using a triple-head rotating gamma camera Prism 3000 (Picker International, Cleveland, Ohio, USA) equipped with low-energy, ultra-high-resolution fan beam collimators. The resulting data were processed using Odyssey software. Images were obtained under the following conditions: 140 keV energy, 15% window, 4-degree steps, 90 directions, 30 s per direction, and a 128 × 128 matrix. The spatial resolution of the scanner was 3.8 mm full-width-at-half-maximum (FWHM). The entire imaging process required about 20 min to perform. All SPECT data were reconstructed using a three-dimensional post-filter (Butterworth) with a cut-off frequency of 0.24 cycles/pixel and an order of 4.0. Chang's method was used to correct the data for absorption (Chang, 0.09/cm). Transverse images, with a slice thickness of 1.72 mm, were obtained parallel to the OM line.

SPM

One disadvantage of SPECT images is that the sizes or sites of hypoperfused areas are not clearly represented, making their comparison with other images difficult. To overcome this disadvantage, we used the statistical parametric mapping (SPM) software (SPM 96 for Windows, Wellcome Department of Cognitive Neurology, London, UK). We conducted the Jackknife test with a normal database for many people, and projected statistically significantly hypoperfused areas onto the standardized brain. In this way, it was possible to objectively represent the sites and sizes of hypoperfused areas.

Data from 36 normal volunteers (10 males and 26 females, age range 20–67 years, mean age 44.4 years) were used as the normal database. These healthy volunteers were free of neurological or psychiatric illness (including alcoholism, drug addiction, atypical headaches, head trauma with disturbed consciousness, and asymptomatic cerebral infarction detectable on T_2-weighted MR images). Informed consent was obtained from all the healthy volunteers. The study was approved by the Ethics Committee of our university.

Each SPECT image was spatially normalized to the stereotaxic space of the Montreal Neurological Institute brain, in order to remove inter-individual morphological differences. The spatial normalization included both affine transformations and a linear combination of smooth spatial basis functions (7 × 8 × 7 mm) for modeling global nonlinear differences in shape. The spatially normalized structural images were resliced to a final voxel size of approximately 2 × 2 × 2 mm^3.

After conversion, the images were smoothed with a 12-mm FWHM Gaussian filter to increase the signal/noise ratio. To examine regional differences, the images were scaled to a mean global cerebral blood flow of 50 ml/100 g/min.

The differences in relative rCBF per voxel were tested by the t-test. The t value was subjected to z conversion so that the mean and standard deviation would become 0 and 1 in the normal distribution, respectively. In this way, areas showing statistically significant differences ($p = 0.001$) were identified. Bonferroni correction ($p = 0.05$) was also performed, considering multiple comparisons. Based on the results of these analyses, changes in the cerebral blood flow following ischemia were projected onto the axial images of the standard brain.

Image Analysis

MRI and SPM studies were evaluated with blinded separate interpretations by two independent radiologists. When the observers did not fully agree, diagnosis was achieved by consensus. The radiologists were blinded to clinical information, such as patient's presenting symptoms.

Lesions in the deep white matter with less blood flow than the cortex are difficult to detect by brain perfusion scintigraphy. That is, scintigraphy is not suitable for evaluation of the progression of cortical infarction towards deeper white matter. In the present study, we compared only the anteroposterior lengths of the infarcts and did not compare the widths, which mainly corresponds to the progress of the infarct in the direction of the deep white matter.

Using SPM, the anteroposterior lengths of significantly hypoperfused areas ($p < 0.001$) were measured, and their percentages relative to the anteroposterior lengths of the cerebral hemisphere (hypoperfusion brain ratio; HBR %) were calculated (fig. 1A).

Also on T_2-weighted MR images, the anteroposterior diameters of hyperintense lesions were measured manually, and their percentages relative to the anteroposterior length of the cerebral hemisphere (infarct brain ratio; IBR %) were calculated (fig. 1B). To exclude the influence of hypoperfused areas appearing anew after the performance of the SPECT, we measured the anteroposterior lengths of only the areas showing scar-like changes and not the surrounding, slightly high-signal intensity areas that did not show signs of scarring, when measuring the anteroposterior lengths of hyperintense lesions on MR images taken more than 1 year after the onset of stroke.

For each infarct, the number of days, which had elapsed after the episode of stroke symptom, was also recorded (table 1). The number of elapsed days was estimated not only for infarcts that were directly responsible for the stroke, and necessitated the MRI and SPECT study, but also for infarcts, which caused previous stroke detected on MR images simultaneously. For the six old infarcts detected in 2 patients, the dates of onset could not be identified, because these patients had not visited our clinic before the onset of the stroke.

Results

When comparing the HBR and IBR within 1 week, no subject had an IBR/HBR ratio between 39 and 75%; therefore, the subjects were divided into a group with a

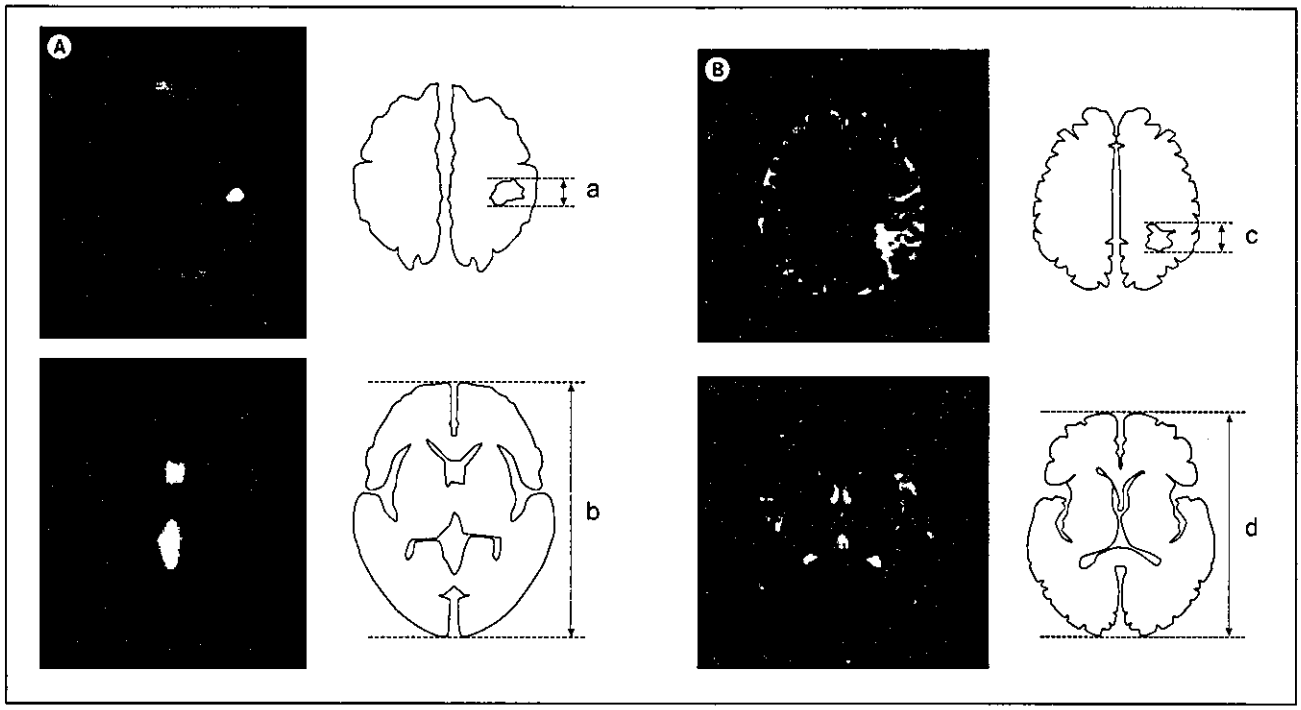

1

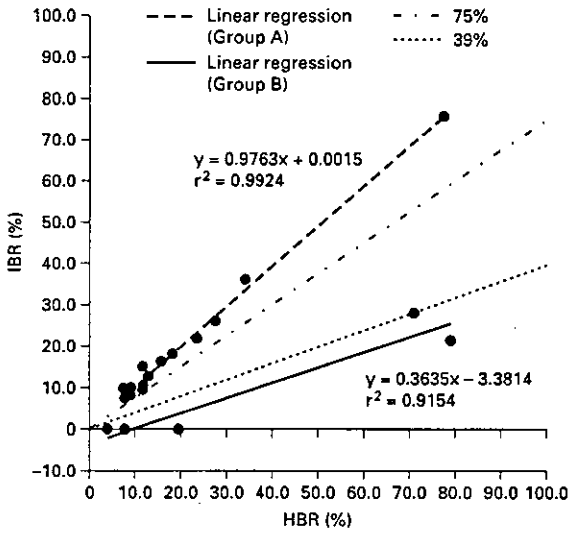

2

Fig. 1. Projection of a significantly hypoperfused area ($p < 0.001$) detected by SPECT onto the standard brain using SPM (**A**). The percentage of the anteroposterior length of the SPM significantly hypoperfused area relative to the anteroposterior length of the cerebral hemisphere (hypoperfusion brain ratio; HBR %) was calculated. Also on T_2-weighted MR images (**B**), the percentage of the anteroposterior length of the hyperintense lesion relative to the anteroposterior length of the cerebral hemisphere (infarct brain ratio; IBR %) was calculated. **A** HBR = a/b × 100(%), **B** IBR = c/d × 100(%).

Fig. 2. Comparison of the HBR with IBR on MRI and SPECT images taken at around the same time. The patients were divided into two groups: group A with a IBR/HBR ratio of over 75% and group B with a ratio below 40%. In group A, the linear regression was defined by Y = 0.976X +0.002 and the multiple correlation coefficient (R^2) was 0.992. In group B, linear regression was defined by Y = 0.364X +3.338 and R^2 was 0.915.

large IBR/HBR ratio (75–125%) and a group with a small IBR/HBR ratio (0–39%), as shown in figure 2. Nine patients (15 lesions) were assigned to group A (large IBR/HBR ratio group), and 5 patients (5 lesions) were allocated to group B (small IBR/HBR ratio group). In group A, a very high correlation was noted between the infarct size and extent of significant hypoperfusion.

When the time-course of changes was followed, infarcts in group A showed little change in size (fig. 3, 5). In group B, all infarcts increased slowly, and after more than

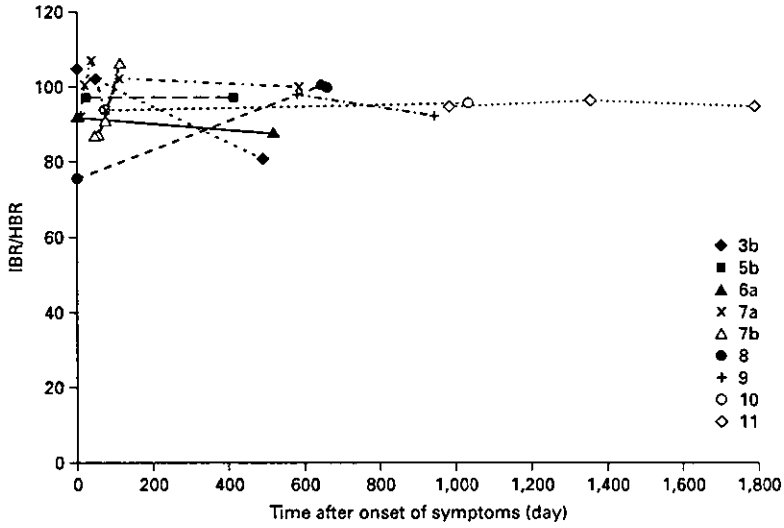

Fig. 3. Time-course of changes in the anteroposterior length of the infarct on T_2-weighted MR images in group A. The Y axis indicates the percentage relative to the surrounding hypoperfused area (IBR/HBR). No significant change in the size of the infarct was noted.

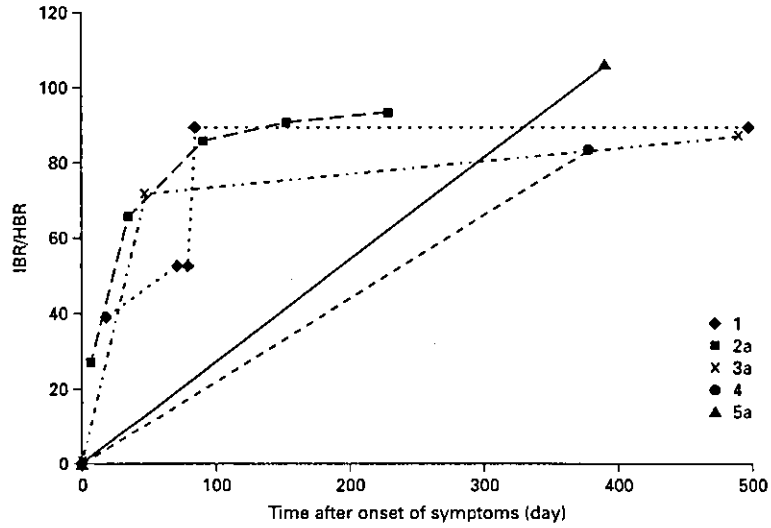

Fig. 4. Time-course of changes in the anteroposterior length of infarcts on T_2-weighted MR images in group A. Each infarct showed a significant tendency of growth. All the infarcts followed for short periods of time showed slow enlargement.

half a year, each IBR/HBR ratio of group B increased to the ratio of group A (75–125%) (fig. 4, 6).

When the relationship between infarction and cerebrovascular disease was analyzed, all patients with infarcts in group B had severe stenosis of the internal carotid arteries bilaterally (table 2). Conversely, of all 7 patients with severe stenosis of the internal carotid arteries of both sides, 5 patients had infarcts in group B. All 4 patients without internal carotid artery lesion had only infarcts assigned to group A.

Table 2. Relationship between bilateral internal carotid artery stenosis and size of infarction in group B

	Group B (+)[1] (n = 5)	Group B (–)[2] (n = 6)
Bilateral ICA stenosis (+) (n = 7)	5	2
ICA stenosis (–) (n = 4)	0	4

[1] Patients with infarcts in group B.
[2] Patients without infarcts in group B.

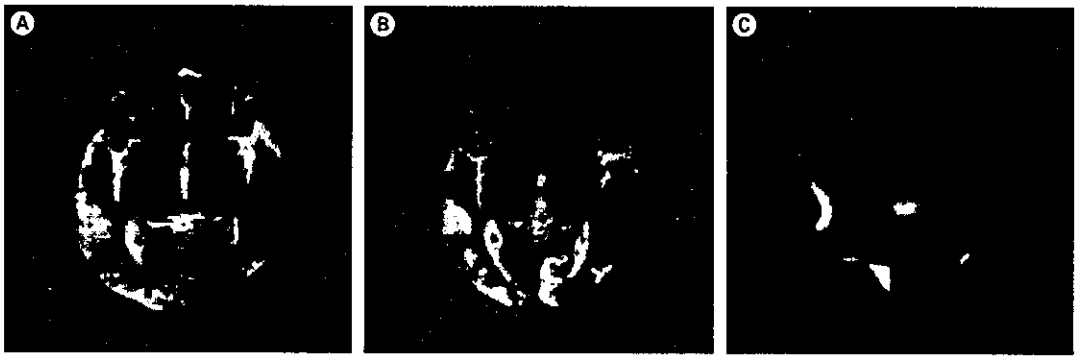

Fig. 5. One-year-old girl with moyamoya disease (group A). Admitted for detailed examination and treatment. On the day following EDAS, the patient developed left-sided hemiplegia. SPECT conducted 23 days after the onset revealed a broad hypoperfused area in the right MCA through the PCA region (**C**). Partially hypoperfused areas were also seen in the left watershed region. T_2-weighted MRI, conducted 24 days after onset, disclosed an infarct approximately identical with the hypoperfused area (**A**). T_2-weighted MRI on the 414th day showed no marked change in the infarct size in the said region (**B**). The new infarct seen in the left PCA region seems to have developed during the follow-up period.

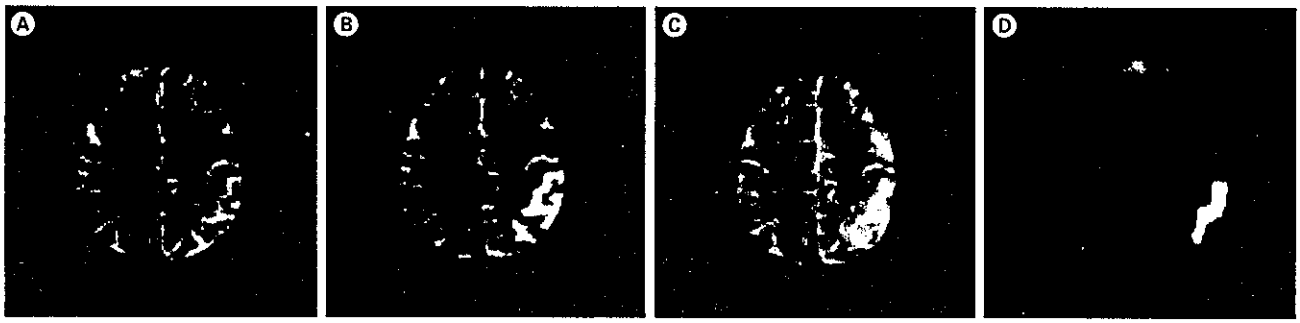

Fig. 6. A 23-year-old woman with moyamoya disease (group B). Admitted after development of hemiplegia on the right side. T_2-weighted MRI conducted 18 days after the onset revealed a slightly high-intensity area around the left angular gyrus (**A**). SPECT conducted on the 22nd day showed a surrounding hypoperfused area with an anteroposterior length three times that of the said region (**D**). MRI on the 72nd day revealed a tendency towards enlargement (**B**). The final infarct (on the 498th day) was approximately identical with the significantly hypoperfused area visible on the initial SPM (**C**). On the 77th day, the patient was treated surgically by bilateral EDAS.

The relationship between the slow enlargement of the infarcts and the clinical symptoms cannot be represented as a numerical value because of the retrospective nature of this study. However, the clinical records of 4 of the 5 patients with infarcts in group B showed that a clinical exacerbation of symptoms (thought to be caused by the infarct) was observed during the period when the infarcts were increasing in size. Since the 1 remaining patient had a PCA territory infarct and aphasia, a clear exacerbation of her symptoms was not seen.

Discussion

In cases of acute ischemic stroke, the infarcted core is usually surrounded by hypoperfused tissue. This abnormally perfused area is considered to be 'tissue at risk', and is called 'ischemic penumbra', if the abnormality is reversible [5, 12, 13]. In the present study, the size of the infarct in many cases was equal to the size of the area showing significant hypoperfusion on the first MR images, while some infarcts were much smaller than the

hypoperfused area. What does the presence of such a broad hypoperfused area around an infarct imply?

In the present study, broad hypoperfusion was seen in 5 cases. In all of these 5 cases, severe stenosis or occlusion of the internal carotid arteries was noted bilaterally. Neumann-Haefelin et al. [14] also reported that the size of the perfusion-weighted image (PWI)/diffusion-weighted image (DWI) mismatch was much greater in patients with severe lesions of the internal carotid artery than in patients not showing carotid artery stenosis. In these cases, collateral flow probably develops as a result of persistence of severe internal carotid artery lesions. It seems therefore likely that even when thromboembolism has taken place, collateral flow, mainly via the circle of Willis, partially compensates for the local follow obstruction at the site of stenosis. Among other possible factors, it seems likely that thrombi in cases of carotid artery stenosis are smaller than those in patients with a cardiac source of the emboli, causing less severe ischemia.

The sizes of the infarcts did not change with time in the group in which the infarct size was the same as the surrounding area showing significant hypoperfusion. On the other hand, in the group of patients showing broader hypoperfused areas, the rate to the hypoperfused area of infarct increased, and after more than half a year, turned into the same rate as the former group. All of the infarcts followed up for short periods of time showed only slow growth, taking more than a month to grow to a size of about 75% of the size of the surrounding hypoperfused area.

Regarding the growth of infarcts, it is often said that the size reaches a peak within 1 week, more significantly during the first 3 days after the onset of stroke [1]. It is also known that some infarcts continue to grow thereafter [2].

In the study conducted by Du et al. [15] using rats, infarction due to severe ischemia (lasting for 90 min) was completed within a day, while infarction due to moderate ischemia (lasting for 30 min) took about 2 weeks to grow to a size equivalent to the peak size of the infarct caused by severe ischemia. In the latter case, apoptosis rather than ordinary necrosis may contribute to the growth of the infarct [2, 15]. In the present study, all patients showing a slow growth of the infarct had severe stenosis of the internal carotid artery bilaterally. It is highly possible that in these patients, continued moderate ischemia, instead of severe ischemia caused by embolism, etc., was operative. The involvement of apoptosis is also possible in these cases.

However, the very slow growth of infarcts observed in this study cannot be fully explained by these factors alone. It seems possible that in addition to continuous mild ischemia around the infarct, other factors may be involved in delayed infarct enlargement, including: (a) possible repetition of embolism at the stenosed site, (b) reduction in the cerebral circulatory reserve, and (c) effects of antiplatelet or anticoagulation therapy administered soon after the onset of stroke.

In the present study, all infarcts surrounded by broad areas of hypoperfusion grew for more than half a year to a size equal to the size of the initial hypoperfused area. This suggests that the hypoperfused tissue around an infarct, as detected on SPM, does not eventually survive, even though much time is taken until this area loses all viability. Are there any therapeutic means that can prevent the enlargement of infarcts?

It has been suggested that more infarcts in the penumbra region can be prevented by intra-arterial fibrinolytic therapy than by standard heparin therapy [16]. In the present study, many patients had undergone urokinase therapy in the very acute stage of the disease. However, since pretreatment SPECT images for these patients were unavailable, we could not evaluate the effects of this therapy.

All of our patients received antiplatelet or anticoagulation therapy in the acute stage of the disease. Of the 5 patients in whom the infarcts showed a tendency towards further growth, 3 were treated surgically. We could not confirm in any case whether or not surgical or medical treatment could prevent the progression of infarction to the hypoperfused area.

Some investigators reported that the volume of the penumbra, which did not advance into infarction in the acute stage, was closely related to subsequent neurological recovery [6, 17]. This suggests that neuronal reorganization may take place in the noninfarcted surrounding area. However, the present study suggests that in many cases, the infarction advances to the hypoperfused areas after a relatively long period of time; simultaneous with the infarct's extension, the clinical exacerbation of symptoms thought to be caused by the infarct is often seen. The relationship between this slow enlargement of the infarcts and the course of neurological findings needs further study.

This study has several limitations. First, the age distribution of the patients was broader than that of the normal SPM database, and especially child data was not contained in the contrast group. However, it was morally impossible to have created a child's normal database.

Second, in this study the sizes of the infarcts and the hypoperfused areas were measured as the anteroposterior length, which is not necessarily related to changes in the

volume. For example, it is possible that persistence of infarction can result in scar-like changes, associated with a decrease in volume due to slit-shaped contraction. This change is not reflected in the anteroposterior length.

Third, the present study was a retrospective study, and SPECT images were obtained at varying points of time after the onset of stroke (in the acute stage in some cases and in the subacute stage in others). Furthermore, follow-up SPECT images were not available for the patients. For these reasons, the time-course of changes in the sizes of the hypoperfused areas could not be followed. Moreover, the intervals between the initial MRI and SPECT assessments ranged from the same day to 7 days apart, so the SPECT imaging results did not necessarily depict the early stage of the perfusion abnormality.

In conclusion, many of the patients with severe bilateral lesions of the carotid artery had broad hypoperfused areas around the infarcts. The infarction progressed to these hypoperfused areas after long periods of time. These results indicate that patients with stenosis of the internal carotid artery often have slowly growing infarcts, and that SPM is useful for predicting the ultimate size of the infarcts.

References

1 Lansberg MG, O'Brien MW, Tong DC, Moseley ME, Albers GW: Evolution of cerebral infarct volume assessed by diffusion-weighted magnetic resonance imaging. Arch Neurol 2001;58:613–617.

2 Pantano P, Caramia F, Bozzao L, Dieler C, von Kummer R: Delayed increase in infarct volume after cerebral ischemia: Correlations with thrombolytic treatment and clinical outcome. Stroke 1999;30:502–507.

3 Schwamm LH, Koroshetz WJ, Sorensen AG, Wang B, Copen WA, Budzik R, Rordorf G, Buonanno FS, Schaefer PW, Gonzalez RG: Time course of lesion development in patients with acute stroke: Serial diffusion- and hemodynamic-weighted magnetic resonance imaging. Stroke 1998;29:2268–2276.

4 Wittsack HJ, Ritzl A, Fink GR, Wenserski F, Siebler M, Seitz RJ, Modder U, Freund HJ: MR imaging in acute stroke: Diffusion-weighted and perfusion imaging parameters for predicting infarct size. Radiology 2002;222:397–403.

5 Karonen JO, Nuutinen J, Kuikka JT, Vanninen EJ, Vanninen RL, Partanen PL, Vainio PA, Roivainen R, Sivenius J, Aronen HJ: Combined SPECT and diffusion-weighted MRI as a predictor of infarct growth in acute ischemic stroke. J Nucl Med 2000;41:788–794.

6 Furlan M, Marchal G, Viader F, Derlon JM, Baron JC: Spontaneous neurological recovery after stroke and the fate of the ischemic penumbra. Ann Neurol 1996;40:216–226.

7 Watanabe Y, Takagi H, Aoki S, Sassa H: Prediction of cerebral infarct sizes by cerebral blood flow SPECT performed in the early acute stage. Ann Nucl Med 1999;13:205–210.

8 Ueda T, Yuh WT, Maley JE, Quets JP, Hahn PY, Magnotta VA: Outcome of acute ischemic lesions evaluated by diffusion and perfusion MR imaging. AJNR Am J Neuroradiol 1999;20:983–989.

9 Baird AE, Austin MC, McKay WJ, Donnan GA: Sensitivity and specificity of ^{99m}Tc-HMPAO SPECT cerebral perfusion measurements during the first 48 h for the localization of cerebral infarction. Stroke 1997;28:976–980.

10 Barber PA, Darby DG, Desmond PM, Yang Q, Gerraty RP, Jolley D, Donnan GA, Tress BM, Davis SM: Prediction of stroke outcome with echoplanar perfusion- and diffusion-weighted MRI. Neurology 1998;51:418–426.

11 Hirano T, Read SJ, Abbott DF, Barid AE, Yasaka M, Infeld B, Barber PA, Davis SM, McKay WJ, Donnan GA: Prediction of the final infarct volume within 6 h of stroke using single photon emission computed tomography with technetium-99m hexamethylpropylene amine oxime. Cerebrovasc Dis 2001;11:119–127.

12 Neumann-Haefelin T, Wittsack HJ, Wenserski F, Siebler M, Seitz RJ, Modder U, Freund HJ: Diffusion- and perfusion-weighted MRI. The DWI/PWI mismatch region in acute stroke. Stroke 1999;30:1591–1597.

13 Hossmann KA: Viability thresholds and the penumbra of focal ischemia. Ann Neurol 1994;36:557–565.

14 Neumann-Haefelin T, Wittsack HJ, Fink GR, Wenserski F, Li TQ, Seitz RJ, Siebler M, Modder U, Freund HJ: Diffusion- and perfusion-weighted MRI: Influence of severe carotid artery stenosis on the DWI/PWI mismatch in acute stroke. Stroke 2000;31:1311–1317.

15 Du C, Hu R, Csernansky CA, Hsu CY, Choi DW: Very delayed infarction after mild focal cerebral ischemia: A role for apoptosis. J Cereb Blood Flow Metab 1996;16:195–201.

16 Klotz E, Konig M: Perfusion measurements of the brain: Using dynamic CT for the quantitative assessment of cerebral ischemia in acute stroke. Eur J Radiol 1999;30:170–184.

17 Mounts JM, Modell JG, Foster NL, DuPree ES, Ackermann RJ, Petry NA, Bluemlein LE, Kuhl DE: Prognostication of recovery following stroke using the comparison of CT and technetium-99m HM-PAO SPECT. J Nucl Med 1990;31:61–66.

Article

Low Dopamine D_2 Receptor Binding in Subregions of the Thalamus in Schizophrenia

Fumihiko Yasuno, M.D., Ph.D.

Tetsuya Suhara, M.D., Ph.D.

Yoshiro Okubo, M.D., Ph.D.

Yasuhiko Sudo, M.D., Ph.D.

Makoto Inoue, M.D., Ph.D.

Tetsuya Ichimiya, M.D., Ph.D.

Akihiro Takano, M.D., Ph.D.

Kazuhiko Nakayama, M.D., Ph.D.

Christer Halldin, Ph.D.

Lars Farde, M.D., Ph.D.

Objective: Several structural and functional brain imaging studies have pointed to a disturbance of thalamic subnuclei in patients with schizophrenia. The dopamine hypothesis of schizophrenia has, however, not been thoroughly examined in terms of this complex structure, which has connections with most brain regions of central interest in schizophrenia research. The aim of the present study was to examine dopamine D_2 receptor binding in subregions of the thalamus in patients with schizophrenia.

Method: The authors used positron emission tomography and the radioligand [^{11}C]FLB457 to examine dopamine D_2 receptor binding in thalamic subregions of 10 drug-naive patients with schizophrenia. Binding potential was calculated by the reference tissue method and used as an index for dopamine D_2 receptor binding. Comparisons were made with 19 healthy subjects. Subregions of interest were defined on individual magnetic resonance images using a percentage-based operational approach. Clinical symptoms were rated by using the Brief Psychiatric Rating Scale (BPRS).

Results: The [^{11}C]FLB457 binding potential was lower in the central medial and posterior subregions of the thalamus in patients with schizophrenia. At a functional level, there was a significant negative correlation between binding potential and BPRS positive symptom scores.

Conclusions: The subregions with low D_2 receptor binding comprise primarily the dorsomedial nucleus and pulvinar, two important components in circuitries previously suggested in the pathophysiology of schizophrenia. Aberrant dopaminergic neurotransmission in thalamic subregions might be a mechanism underlying positive symptoms in schizophrenia.

(Am J Psychiatry 2004; 161:1016–1022)

The dopamine D_2 receptor has long been of central interest in research on the pathophysiology of schizophrenia. Early positron emission tomography (PET) studies focused on the striatum, a region with a high density of D_2 receptors. Improvements in PET methodology now allow the examination of low-density dopamine D_2 receptor populations in several limbic and cortical regions in which structural or biochemical abnormalities have been reported in schizophrenia. In a recent analysis of cortical and subcortical regions, we found low radioligand binding to dopamine D_2 receptors in the anterior cingulate cortex of patients with schizophrenia and a correlation with positive symptom scores (1).

On the other hand, functional abnormality of schizophrenia has also been discussed in terms of thalamic circuitry (2). Imaging studies have consistently revealed smaller thalamic volumes in patients with schizophrenia as well as altered thalamic perfusion and metabolism (2–13). Neuropathological studies have found a reduction in the number of neurons in the mediodorsal nucleus of the thalamus in schizophrenia brains (14–17). Schizophrenia-associated neuronal loss has also been found in the pulvinar (17). A synapse-related protein study reported that the thalamic abnormalities include synaptic disturbances (18).

The thalamus was not included in early maps showing dopaminergic innervation in the rodent brain (19). However, dopamine D_2 receptors have more recently been identified in the human thalamus in vitro (20, 21) and in vivo using PET (22–24). The possibility that dopamine D_2 receptors in the thalamus are involved in the therapeutic actions of antipsychotics has been supported by PET studies that demonstrated dopamine D_2 receptor occupancy in the thalamus by antipsychotic drugs (25). Each of the major 23 subnuclei of the thalamus (26) has a unique set of efferent and afferent projections with different functional implications. In a previous study, we found a tendency toward low density of dopamine D_2 receptors in the thalamus (1). However, in that study we focused on the thalamus as a whole and did not take its detailed complexity into account.

The aim of the present PET study was to examine separately dopamine D_2 receptor binding in five major subregions of the thalamus. Ten neuroleptic-naive patients with schizophrenia and 19 healthy comparison subjects were examined with the radioligand [^{11}C]FLB457, a substituted benzamide with a very high affinity for dopamine D_2 re-

ceptors (27). We then investigated whether there were correlations between subregional binding and psychopathology score as assessed with the Brief Psychiatric Rating Scale (BPRS) (28).

Method

Subjects

This study was approved by the Ethics and Radiation Safety Committee of the National Institute of Radiological Sciences, Chiba, Japan. After complete description of the study, written informed consent was obtained from all subjects. The patients were recruited from the outpatient units of five university-affiliated psychiatric hospitals and the psychiatric divisions of general hospitals in the prefectures of Tokyo and Chiba. Ten drug-naive right-handed male patients with schizophrenia (mean age=29.5 years, SD=7.8) who met DSM-IV criteria for schizophrenia or schizophreniform disorder were included. One patient satisfying the criteria for schizophreniform disorder (duration of illness was 1 month at the time of study entry) met the criteria for schizophrenia at 6-month follow-up. His behavioral ratings were evaluated at the time of study entry. Eight of the 11 patients in a previous study (1) had been examined with magnetic resonance imaging (MRI) and could thereby be included in the present analysis that also included two newly recruited patients. The other three patients had refused to participate in the MRI scan (1), and we could not include them in the present analysis. The duration of illness ranged from 1 month to 7 years, with a median of 2 years. Psychopathology was assessed by the 18-item Oxford version of the BPRS translated into Japanese (item score range=0–6 points) (28). Sum scores for positive and negative symptoms were calculated (1, 29), with the positive symptom subscale including the following eight items: conceptual disorganization, mannerisms and posturing, hostility, grandiosity, suspiciousness, hallucinatory behavior, unusual thought content, and excitement. The negative symptom subscale included these three items: emotional withdrawal, motor retardation, and blunted affect. BPRS total scores ranged from 14 to 42 (mean=29.3, SD=8.9), the mean positive symptom score was 14.6 (SD=4.6), and the mean negative symptom score was 5.5 (SD=4.6). The healthy subjects were recruited through notices on bulletin boards at universities and their affiliated hospitals where the patients were diagnosed. The 19 healthy right-handed male comparison subjects were age-matched (mean=29.6 years, SD=7.5). Parental socioeconomic status was determined on the basis of the Hollingshead-Redlich scale, and no significant differences between patients (mean=2.6, SD=0.7) and comparison subjects (mean=2.3, SD=0.5) were found ($t=1.30$, $df=27$, $p>0.20$). The comparison subjects did not meet criteria for any psychiatric or neurological disorder and had no first-degree relatives with neuropsychiatric disorders.

PET and MRI Procedures

The PET system ECAT EXACT HR+ (CTI-Siemens, Knoxville, Tenn.) was used to measure radioactivity in the brain. The field of view of this system is 15.5 cm. To minimize head movement, a head fixation device (Fixster, Stockholm) was used. A transmission scan for attenuation correction was performed using a ^{68}Ge-^{68}Ga source. Acquisitions were performed in three-dimensional mode with the interplane septa retracted. A bolus of 89.5–249.0 MBq (mean=172.5, SD=40.0) of [^{11}C]FLB457 with high specific radioactivity (64.9–534.9 GBq/μmol) was injected intravenously into a cannula inserted in an antecubital vein. The cannula was then flushed by the rapid injection of 20 ml of saline. Radioactivity in brain was measured in a series of scans for 80 minutes starting immediately after the injection. The emission scans were reconstructed with a Hanning filter cutoff frequency of 0.4 (full width at half maximum=7.5 mm). Images from the reconstructed volume were displayed as 67 horizontal sections. MR images were acquired on a Phillips Gyroscan NT, 1.5 tesla. T_1-weighted images of the brain were obtained to allow for differentiation between white and gray matter. The scan parameters for 1-mm-thick, three-dimensional T_1 images in the transversal plane were as follows: TR/TE=19/10 msec, flip angle=30°, matrix=256×256, field of view=256×256 mm, number of excitations=1.

Quantitative Analysis of [^{11}C]FLB457 Binding

Quantitative analysis was performed using the three-parameter simplified reference tissue model (30, 31). The cerebellum was used as a reference region because it has been shown to be almost devoid of D_2 receptors (23, 31). The model provides an estimation of the binding potential, which is defined by the following equation:

$$BP=k_3/k_4=f_2\,B_{max}/\{K_d\,[1+\Sigma_i\,F_i/K_{di}]\},$$

where k_3 and k_4 describe the bidirectional exchange of tracer between the free compartment and the compartment representing specific binding, f_2 is the "free fraction" of nonspecifically bound radioligand in brain, B_{max} is the receptor density, K_d is the equilibrium dissociation constant for the radioligand (32), and F_i and K_{di} are the free concentration and the dissociation constant of competing endogenous dopamine, respectively. The model also provides the parameter R_1, which represents the ratio of radioligand delivery in the region of interest to that in the reference region (influx ratio).

Thalamic Subdivisions

Regions of interest for five operationally defined subregions of the thalamus were defined on MR images according to a manual tracing technique that has been described in the literature and applied previously for the study of thalamic volumes in schizophrenia (5, 7). The regions of interest were delineated three-dimensionally on MR images and displayed by a distinct color as described previously (33) (Figure 1).

In the first step, the boundaries of the whole thalamus were identified. The mamillary body was used as the anterior boundary. The internal capsule was the lateral boundary, the third ventricle the medial boundary, and the inferior border of the third ventricle the inferior boundary. The posterior boundary was defined as the location where the hemispheres of the thalamus merged under the crux fornix. The superior boundary was the main body of the lateral ventricle (7). In the second step, the thalamus was subdivided into five distinct regions. The thalamus was first divided into medial and lateral parts. A line drawn parallel to the lateral border of the midbrain, the interhemispheric fissure, and the cerebral aqueduct represented the vertical bisection (coronal view in Figure 1). This line was continued through all thalamic slices to create a plane of bisection parallel to the interhemispheric fissure. The individual number of contiguous coronal slices in which the thalamus appeared was then calculated.

The thalamus was divided into anterior, central, and posterior divisions that were defined as fixed percentages of the total number of coronal slices. The anterior and central divisions each contained 40% of the total number of slices, and the posterior division contained 20%. Using this approach, the thalamus was divided into six subregions. The medial and lateral portions of the posterior thalamus were then combined, since they both corresponded to the pulvinar (axial view in Figure 1). In the final step, the regions of interest were linearly transformed using the parameters obtained from the coregistration of the individual MRI and PET images. This was done using SPM 99 (34), with the default parameter option of mutual information (35). After transformation of the regions of interest from MRI to PET, the regional radioactivity of each region of interest was calculated for each frame, corrected for decay, and plotted against time. The average values for

FIGURE 1. Thalamic Subdivisional Regions of Interest[a]

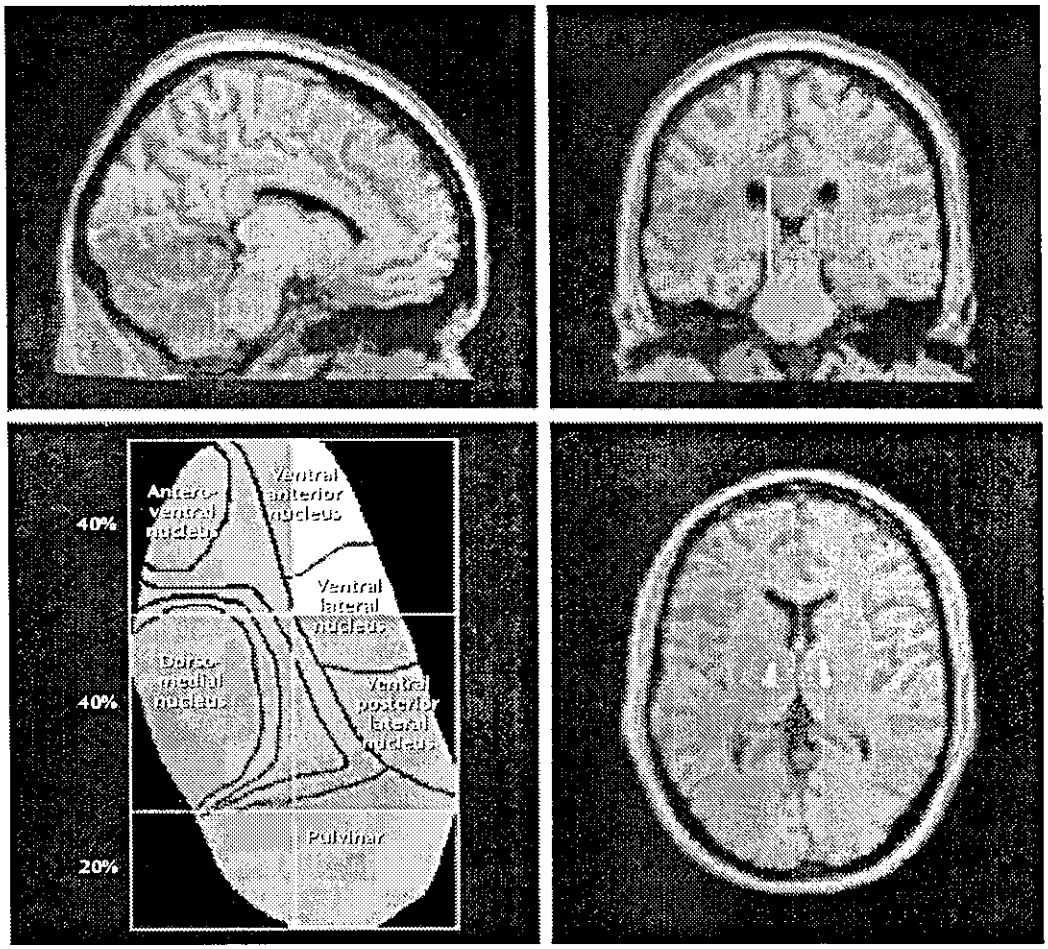

[a] Regions of interest were defined on T_1-weighted MR images by a manual tracing technique as described in a previous article examining the thalamic volumes in schizophrenia (7). Approximate regions of specific thalamic nuclei are depicted in the representation of the axial view of the thalamus (lower left) (5, 7). The line drawn in the coronal view of the MRI—which is parallel to the lateral border of the midbrain, interhemispheric fissure, and cerebral aqueduct—represents the line of vertical bisection of each thalamus.

regions of interest in the right and left hemisphere were used to increase the signal-to-noise ratio for the calculations. Subdivision of the thalamus and measurement of binding potential values was performed in duplicate by a single investigator (E.Y.) in 10 of the healthy subjects, and intrarater reliability was assessed. High intraclass correlations (ICCs) for subregions were seen for the two sets of measurements (anterior medial: ICC=0.96, anterior lateral: ICC=0.94, central medial: ICC=0.92, central lateral: ICC=0.90, posterior: ICC=0.82).

Morphological analysis was performed on the volume of the region of interest defined on MRI images. The size of the area was calculated, summed across slices, and multiplied by the slice thickness (1 mm), yielding approximate volumes. Intracranial volume was used as a covariate when comparing volumetric measures between the groups.

Statistical Comparisons

The binding potential and influx ratio (R_1) values for the whole thalamus were compared between patients and healthy subjects by Student's t test. The volumes for the whole thalamus were compared between patients and comparison subjects using one-way analysis of covariance (ANCOVA) with the intracranial volume as covariate. Group differences in the binding potential values of the thalamic subregions were compared by using multivariate analysis of variance (MANOVA). Follow-up serial one-way analyses of variance (ANOVAs) were performed to specify regional differences. To examine the influence of regional differences of blood flow and volumes on those of the binding potential values, serial one-way ANOVAs and ANCOVAs with intracranial volume as covariate were performed to specify regional differences of the influx ratios and volumes, respectively. A p value of 0.05 (two-tailed) was chosen as the significance threshold. The relationship between regional binding potential values and BPRS scores (total score as well as positive and negative symptom subscale scores) was evaluated in the correlation analysis. In consideration of the effect of the duration of illness, we examined the relationship of its variables to regional binding potential values. We also evaluated the relationships of age and parental socioeconomic status to the binding potential values in healthy subjects and patients. In the correlation analysis, we used the Pearson correlation method, and $p<0.01$ [0.05/5] was considered as significant to avoid type I errors due to the multiplicity of statistical analyses.

TABLE 1. [^{11}C]FLB457 Binding Potential[a] in Thalamic Subregions of Patients With Schizophrenia and Healthy Comparison Subjects

Thalamic Subregion	Binding Potential[b]					
	Healthy Subjects (N=19)		Schizophrenia Patients (N=10)		Analysis of Variance	
	Mean	SD	Mean	SD	F (df=1, 27)	p
Anterior medial	3.72	0.70	3.67	0.23	0.05	0.83
Anterior lateral	2.69	0.51	2.55	0.25	0.69	0.41
Central medial	3.95	0.48	3.53	0.43	5.21	0.03
Central lateral	2.56	0.38	2.43	0.28	0.84	0.37
Posterior	2.64	0.26	2.33	0.23	10.15	0.004

[a] Index of dopamine D_2 receptor binding.
[b] Multivariate analysis of variance was performed to test for group differences between comparison subjects and patients (Wilks's lambda=0.56; F=3.64, df=5, 23, p=0.01).

Results

With regard to the binding potential values for [^{11}C]FLB457 binding in the whole thalamus, there was no significant difference between the two groups (schizophrenia patients: mean=3.31, SD=0.33; comparison subjects: mean=3.54, SD=0.45) (t=1.45, df=27, p>0.15). However, multivariate analyses of the binding potential values in the thalamic subregions showed significant differences between patients with schizophrenia and comparison subjects. Follow-up ANOVAs revealed that the binding potential values in the central medial region and the posterior region were significantly lower in the patients (Table 1, Figure 2).

The influx ratio (R_1) for the whole thalamus (schizophrenia patients: mean=0.84, SD=0.50; comparison subjects: mean=0.87, SD=0.57) did not differ significantly between patients and comparison subjects (t=1.62, df=27, p>0.12) nor did it differ in any subregion (Table 2). The volume of the whole thalamus was not significantly different between patients (mean=8.65, SD=1.16) and healthy subjects (mean=8.65, SD=1.19) (F=0.005, df=1, 26, p>0.94), and no significant difference was found for any of the thalamic subregions (Table 2).

For the central medial region and the posterior region there was a statistically significant negative correlation between binding potential and positive symptom subscores on the BPRS (Table 3, Figure 3). There was no significant correlation between binding potential and the BPRS total scores or negative symptom subscore for any region. Further, no significant relationship was observed between regional binding potential values and the duration of illness, age, or parental socioeconomic status in comparison subjects and patients.

Discussion

In a previous PET study, we reported low dopamine D_2 receptor binding in the anterior cingulate in patients with schizophrenia and a statistical trend for low binding in the thalamus (1). In the present study with a partly overlapping patient group, a more detailed analysis of the thalamus indicated low [^{11}C]FLB457 binding potential in the central medial and posterior subregions of the thalamus in patients with schizophrenia. Highly elevated levels of dopamine have been found postmortem in the thalamus of schizophrenia (36), and the reduction in binding could be attributed to an increase in endogenous dopamine. However, our previous study indicated that extrastriatal [^{11}C]FLB457 was not sensitive to endogenous dopamine, as [^{11}C]FLB457 binding in the cortex and thalamus was not significantly affected by a 1-mg/methamphetamine challenge (37). Therefore, the present findings may be attributed to the receptor density. A longitudinal study will be required to settle the issue of whether low density is acquired during the course of disease or whether it represents abnormal brain development (38).

The subregions with low D_2 receptor binding comprise primarily the dorsomedial nucleus and pulvinar, two important components in circuitries previously suggested in the pathophysiology of schizophrenia (5, 7). The thalamus has long been suggested to have a gating function that filters the sensory input to the cortex, thereby providing protection against sensory overload and hyperarousal (39). Startle prepulse inhibition, a sensitive measure of sensory gating, has indeed been suggested as being related to dopamine neurotransmission in the thalamus (40). Both animal and human studies have provided evidence that the mediodorsal thalamus has a particular role in the regulation of startle prepulse inhibition (41–43). In experimental studies, it has been shown that prepulse inhibition of startle can be disrupted after microinjection of the dopamine

FIGURE 2. [^{11}C]FLB457 Binding Potential in the Central Medial and Posterior Subregions of the Thalamus in Patients With Schizophrenia (N=10) and Healthy Comparison Subjects (N=19)[a]

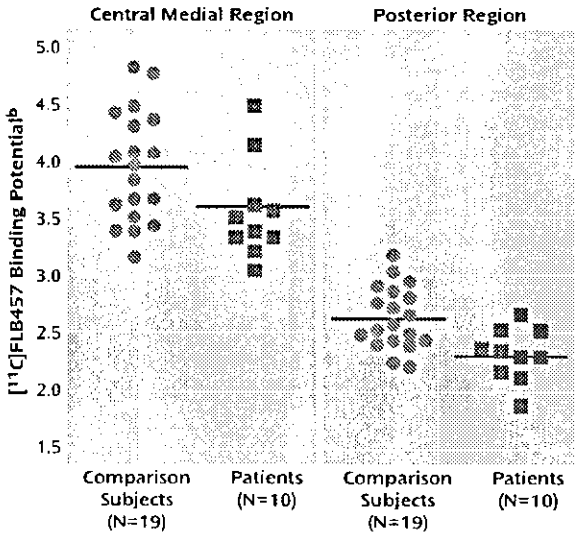

[a] The horizontal line represents group mean.
[b] Index of dopamine D_2 receptor binding.